### SPECIAL ISSUE ARTICLE



# Enthalpy relaxation of sodium aluminosilicate glasses from thermal analysis

Brittney M. Hauke 💿 📗 John C. Mauro 💿

Department of Materials Science and Engineering, The Pennsylvania State University, University Park, Pennsylvania, USA

### Correspondence

Brittney M. Hauke, Department of Materials Science and Engineering, The Pennsylvania State University, University Park, PA 16802, USA.

Email: bmh58@psu.edu

### Funding information

National Science Foundation, Grant/Award Number: DMR 1928546

### **Abstract**

The sodium aluminosilicate (NAS) glass family is important for many different industrial applications, but glass relaxation has not yet been thoroughly studied in this system. Thermal analysis techniques such as differential scanning calorimetry (DSC) and modulated differential scanning calorimetry (MDSC) can provide insight into the enthalpy relaxation of glass by measuring the glass transition temperature  $(T_g)$ , activation energy, and enthalpy of relaxation. MDSC is mostly used to study nonoxide and low  $T_{\rm g}$  glasses, and there is much debate about whether the nonreversing heat flow analysis method is accurate. To the authors' knowledge, this is the first paper using MDSC to study these NAS compositions, and one of few papers to report MDSC on high  $T_{\rm g}$  oxide glasses. We report on one set of modulation conditions that obtain a linear response using Lissajous curves, as well as comparing the activation energy calculated from DSC with the enthalpy of relaxation obtained from MDSC. Our results show that the activation energy and enthalpy of relaxation do not give the same compositional minimum in relaxation, and therefore more work is needed to investigate the validity of the nonreversing heat flow approach for high  $T_{\rm g}$  oxide glasses.

### KEYWORDS

thermal analysis, glass transition, activation energy, silicates, glass-forming systems

# 1 | INTRODUCTION

One of the most important glass compositions for industrial applications is the sodium aluminosilicate (Na<sub>2</sub>O–Al<sub>2</sub>O<sub>3</sub>–SiO<sub>2</sub>) or NAS family, which after undergoing an ion exchange treatment, are used as protective coverings for screens and windshields. <sup>1,2</sup> During both the annealing heat treatment and ion exchange process, the glass undergoes some amount of relaxation toward the supercooled liquid state. <sup>3</sup> This relaxation is the subsequent lifting of constraints frozen in during cooling through the glass tran-

sition region and is an inherent property of all glasses due to their nonequilibrium nature. At room temperature, the relaxation phenomenon appears to be frozen to an outside observer over short time scales.<sup>4</sup>

Relaxation impacts all glasses and is important for industrial applications. At higher temperatures, such as during a heat treatment for fabrication, or over a very long time scale, measurable relaxation can be observed.<sup>5</sup> It is also spontaneous and can involve viscous flow, causing aging of glasses andthus changing the structure and properties. Many compositions used in industrial glass families

This is an open access article under the terms of the Creative Commons Attribution-NonCommercial License, which permits use, distribution and reproduction in any medium, provided the original work is properly cited and is not used for commercial purposes.

© 2024 The Author(s). International Journal of Applied Glass Science published by American Ceramics Society and Wiley Periodicals LLC.

Int J Appl Glass Sci. 2024;1–11. wileyonlinelibrary.com/journal/ijag

20411294, 0, Downloaded from https://ceramics.onlinelibrary.wiley.com/doi/10.1111/jag.16688 by Pennsylvania State University, Wiley Online Library on [28/10/2024]. See the Terms and Conditions (https://onlinelibrary.wiley

1-conditions) on Wiley Online Library for rules of use; OA articles are governed by the applicable Creative Commons Licenso

contain multiple network forming oxides (SiO<sub>2</sub>, Al<sub>2</sub>O<sub>3</sub>, B<sub>2</sub>O<sub>3</sub>, P<sub>2</sub>O<sub>5</sub>, etc.); therefore, knowing the structural role of each network former and modifier is key to understanding relaxation across different glass families.<sup>6-10</sup> Relaxation also impacts many properties of glasses and is a fundamental behavior of both glasses and polymers. Stress relaxation can compromise the strength of ion-exchanged glass and limits the ion exchange temperature, which in effect keeps the ion exchange process monetarily and temporally costly. 11,12 Structural relaxation impacts a large range of glass properties, including the interdiffusion rate of ions.<sup>4,8</sup> Volume relaxation results in compaction, causing pixel misalignment during manufacturing of substrate panels for liquid crystal displays.<sup>5</sup> Rayleigh scattering, the principle used in glass optical fibers, is a function of thermal history and the relaxation of density fluctuations. 4,13

One of the reasons that relaxation has not been thoroughly investigated in NAS (Na<sub>2</sub>O-Al<sub>2</sub>O<sub>3</sub>-SiO<sub>2</sub>) glasses is because their structure is still being investigated. 14-22 The role of Al in the glass network is currently debated and seems to depend on the ratio of Al to Na (referred to in the literature as  $R = [Al_2O_3]/[Na_2O]$  mol/mol). In the 1960s, NAS glasses were found to exhibit anomalous/unexpected behavior of density, refractive index, and viscosity as a function of alumina to modifier content.<sup>23</sup> This increase in viscosity was observed with a maximum at the ratio of R = 1. Different percentages of SiO<sub>2</sub> also exhibited a shift in the viscosity maximum at R = 1.24For alkali and alkaline earth aluminosilicate glasses, when R < 1 (R = [Al<sub>2</sub>O<sub>3</sub>]/[M], where M is modifier oxide such as Na2O or CaO), modifiers such as Na or Ca ideally charge balance all the negatively charged (AlO<sub>4/2</sub>)<sup>-</sup> tetrahedra. Any excess modifier creates nonbridging oxygens (NBOs) on SiO<sub>2</sub> tetrahedra, leading to a decrease in the network conductivity: this is referred to as the metaluminous region. R = 1 is called the subaluminous, or tectosilicate join, and as R approaches 1, all modifier cations become associated with Al tetrahedra for charge balancing, which should result in a fully connected network with no NBOs.  $^{4,25}$  R > 1 is the peraluminous region, where alumina content exceeds the amount of modifier in the system and requires a mechanism for charge balancing the Alcentered tetrahedra because not enough modifier exists. The structural dispute arises from this charge balancing mechanism above R = 1. There is much discussion in the literature about whether the charge balancing takes place via five- or six-coordinated Al, three-coordinated oxygen (also called triclusters), or a mixture of each. 16,18,21,22,26

Currently, relaxation is being studied in a variety of glass families, particularly calcium aluminosilicates, 27-29 sodium aluminoborosilicates,<sup>30</sup> and chalcogenide systems, 7,13,31 but less work has been devoted to the NAS family and the atomic scale origin of relaxation

remains mostly unknown.<sup>10</sup> Relaxation is challenging to study because different types of relaxation occur on distinct time scales.<sup>8</sup> Additionally, primary relaxation mechanisms may vary under different temperature regimes. 9 An added challenge is that in NAS glasses, the role of Al3+ and Na+ in the structure and its effect on relaxation have not been thoroughly examined.

While differential scanning calorimetry (DSC) has many uses in glass science and beyond, there are several limitations. Specifically, a standard DSC scan signal of the glass transition region is a convolution of multiple dynamic processes. These signals include both a kinetic and thermodynamic contribution to the heat capacity. This is due to dynamic heterogeneities, which are characteristic of supercooled glass-forming liquids, leading to the complex nature of the temperature dependence of the heat capacity as a function of thermal history.<sup>32–35</sup> Temperature-modulated differential scanning calorimetry (MDSC or TMDSC) is the next step and can overcome the limitations of standard DSC. Instead of using a linear heating rate like with DSC, MDSC uses a sinusoidally modulated heating rate, where the heat capacity is measured via applying a small sinusoidal temperature oscillation while the sample is held isothermally. The temperature profile of MDSC is

$$T(t) = T_0 + qt + A_t \sin(\omega t)$$

where  $T_0$  is the initial temperature, q is the heating rate, t is the time, and  $A_t$  and  $\omega$  are the amplitude and angular frequency of the sinusoidal oscillations, respectively. Differentiating the above equation leads to the modulated heating rate

$$\frac{\partial T}{\partial t} = q + A_t \omega \cos(\omega t).$$

The first direct measurement of relaxation behavior using the complex heat capacity was performed on amorphous selenium by Gobrecht et al. in 1971. They used a modified Perkin-Elmer DSC where the temperature was periodically varied using a generator.<sup>36</sup> Then in 1985 Birge and Nagel measured frequency dependence through the glass transition by using a sinusoidal heat flux, which they called specific heat spectroscopy.<sup>37</sup> They showed how both the imaginary and real parts of the heat capacity of glycerol change as a function of temperature and frequency and this idea has been expanded both commercially and to more glass families. It was not until the 1990s that this technique was commercialized with the help from Reading et al.34,35 MDSC has been used to study a variety of glass families, particularly glassy selenium, <sup>7,38</sup> As-Se, <sup>39,40</sup> Ge-Se, 38,40-43 Ge-As-Se, 40 Ge-Te-In-Ag, 44 sodium and potassium silicates, 45 sodium germanates, 46 tellurium

vanadates,<sup>47</sup> lithium borates,<sup>48</sup> sodium phosphates,<sup>49</sup> and most recently calcium aluminosilicates.<sup>28,29,50</sup>

There are two ways to analyze MDSC data to gain insight into relaxation. The first, which is the one demonstrated in this paper, uses the nonreversing heat flow directly measured by the instrument. 32,34,35 This is a less mathematically rigorous method than the second technique, which is to analyze the complex heat capacity, and as such the nonreversing heat flow method is contentious. 32,51-55 The nonreversing heat flow method has been used to study a variety of glass families, especially the chalcogenides and borate containing oxides. 7,31,40,48,56,57 Much of this work has been spearheaded by Boolchand and colleagues and focuses on tying topological constraint theory (TCT) to a minimum in enthalpy relaxation. Boolchand expanded upon the initial TCT by suggesting that isostatic configurations have a defined width and that there is a range of topologically optimized compositions. 41,42,58-60 This range is called an intermediate phase and is attributed to a selforganization of the glassy network, where it attempts to achieve an isostatic condition, even if there are short- or intermediate-range defects. 58,61,62 One way to detect an intermediate phase is via reversibility windows in MDSC, which are minima in the nonreversing enthalpy. 40,41,58–61 Complex heat capacity results for these glasses will be published in a future paper, and authors point to the subsequent references<sup>32,38–44</sup> for more information.

This paper reports glass transition temperatures and densities and investigates enthalpy relaxation in a wide compositional range of NAS glasses by DSC and MDSC. In particular, the glass transition temperatures and activation energy of enthalpy relaxation when calculated from DSC and the nonreversing heat flow method of MDSC are compared. The nonreversing heat flow method is studied here for multiple reasons; first, this method has not been widely used on sodium aluminosilicate glasses or high  $T_g$ oxide glasses. Second, this method still needs to be studied to determine whether it is a valid analysis technique, and third, is the default analysis method used by the TA SDT 650, which was used for these experiments. Expanding our fundamental understanding of relaxation will allow for predicting and designing glasses with a minimum in relaxation, mitigating undesirable changes to structure and creating glasses with improved properties.

# 2 | MATERIALS AND METHODS

# 2.1 | Glass preparation

Compositions were chosen after consulting the phase diagram of the Na<sub>2</sub>O-Al<sub>2</sub>O<sub>3</sub>-SiO<sub>2</sub> system and looking for an area centered around a eutectic for a low enough liquidus

temperature to avoid crystallization.<sup>11</sup> The compositions were synthesized using the appropriate batch materials  $(SiO_2, Al_2O_3, and Na_2CO_3)$  with purities of >99%. Batch materials were combined in Nalgene bottles and shaken for  $\geq$ 5 min for mixing. The compositions were designed with 61 mol%  $SiO_2$  with varying amounts of  $Na_2O$  and  $Al_2O_3$ , including one composition with no  $Al_2O_3$  (a sodium silicate glass). Having a range of  $Al_2O_3$  concentrations allows for investigation into the interplay between Al and Na across the compositional space from R = 0 to 1.42, as seen in Figure 1.

Samples were melted at  $1600-1700^{\circ}$ C for 2 h in 90Pt/10Rh crucibles; all samples were melted at least twice to ensure homogeneity and similar thermal histories. Samples with larger amounts of  $Al_2O_3$  were melted three to four times to overcome the increase in viscosity. For low concentrations of  $Al_2O_3$ , samples were poured onto a stainless-steel plate and air quenched, while for higher  $Al_2O_3$  content, samples were water quenched while still in the crucible and then removed. All compositions were powdered and used for inductively coupled plasma emission spectrometry (ICP-AES), powder x-ray diffraction (XRD), and thermal analysis.

# 2.2 | Characterization methods

NAS glass compositions were validated using ICP-AES; samples were crushed to around 100 mesh (~150 μm) using a standing ceramic pulverizer and analyzed on a Thermo iCAP 7400 ICP spectrometer, using the lithium metaborate dissolution method and rock standards for calibration.<sup>63</sup> All NAS glasses were also analyzed via powder XRD to confirm noncrystallinity, and a selection of compositions (R = .09, R = .38, R = .63, R = 1.05, and R = 1.42) is shown in Figure 3. Samples were again powderized to around 100 mesh and were placed on a Bragg-Brentano HD flat sample stage. XRD was measured using a PANalytical Empyrean system with a Cu-K $\alpha$  x-ray source, from 5° to 60°. Density measurements were done three times on three different samples in water using the Archimedes method via a Mettler Toledo balance. 4 Three different measurements were averaged and used to calculate error, and the average densities are reported in Table 2.

Differential scanning calorimetry (DSC) involves heating an empty reference pan and a sample pan in conjunction and monitoring the heat flow of both as a function of time and temperature. The calorimeter measures the heat absorbed or released by the sample when it undergoes a specific temperature path. As chemical reactions and physical transitions take place, there is an associated exothermic or endothermic reaction of heat, which creates the heat flow signal measured by the DSC.



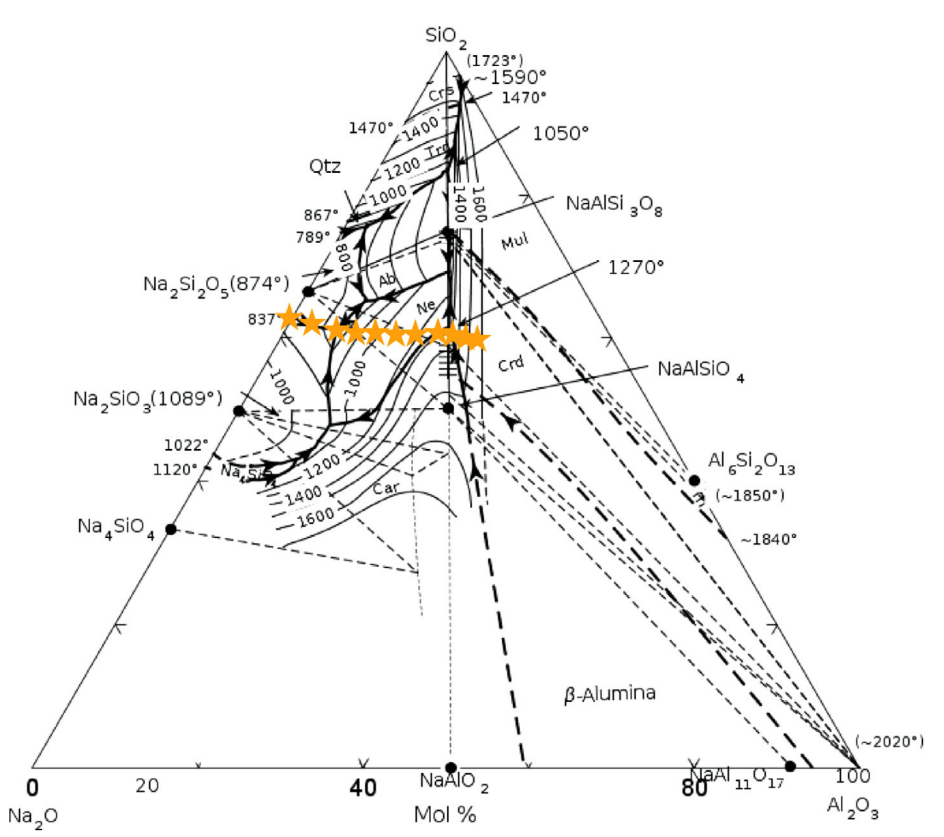


FIGURE 1 Ternary phase diagram of the sodium aluminosilicate system. Stars indicate the glass compositions synthesized and studied in this paper. Phase diagram modified from Osborn E F, Muan A. "System  $Na_2O-Al_2O_3-SiO_2$ ; Composite." Revised and redrawn, "Phase equilibrium diagrams of oxide systems," Plate 4.

All DSC data for the NAS glasses were measured on a TA instrument SDT Discovery 650 at 10°C/min, 20°C/min, 40°C/min, and 60°C/min from 150°C up to 1000°C depending on the glass composition. All samples were powdered and added to alumina sample pans with lids, and sample masses ranged from 20 to 40 mg. The standard SDT 650 calibrations were performed for all heating rates and include a weight calibration, differential thermal analysis (DTA) calibration with empty beams (no reference pan and no sample pan), temperature calibrations and verifications using indium, zinc, and silver standards, cell constant calibration with an indium standard, and heat flow calibrations first using an empty reference and sample pan and then adding a sapphire standard against the empty reference pan. The glass transition temperature  $(T_g)$ was determined by two different methods: the midpoint method used by the TRIOS software and via a geometric representation of DSC data using a python package called TransitionPy. The midpoint method involves finding the onset and end of the glass transition using tangents, where the midpoint or  $T_g$  is determined from the inflection. This technique is part of the TRIOS software and is similar to ASTM E1356–08.<sup>64</sup> The geometric analysis method uses a statistical fitting with high-order polynomial smoothing and peak fitting for precise determination of the onset, inflection, and end temperatures of the glass transition. This is done by analyzing both the first and second derivatives of the DSC curve; the first derivative to determine  $T_{\rm g}$  from the inflection point, and second derivative to determine the onset glass transition temperature.<sup>65</sup>

For modulated differential scanning calorimetry (MDSC), the first challenge is picking the appropriate experimental parameters. First, a nonreversing heat flow calibration is run for the desired heating rate and involves heating an empty reference pan against a sapphire standard at the desired modulation conditions. The user will need to specify a heating rate, oscillation frequency or period, and the temperature amplitude of the oscillation. These choices depend on the equipment and the composition of the glass. The modulation conditions strongly depend on the thermal history and fragility of the glass-forming system in question. 28,32,66 To confirm the modulation conditions are accurate and linearity is preserved, Lissajous curves, which plot the modulated heat flow versus the modulated heating rate, are used. Ideally, the Lissajous curve appears as a diagonal oval shape. 32,67 Figure 2 shows a selection of Lissajous curves from the MDSC measurements reported here, where



2041 1294, 0, Downle

State University, Wiley Online Library on [28/10/2024]. See the Terms

ions) on Wiley Online Library for rules of use; OA articles are governed by the applicable Creative Comm

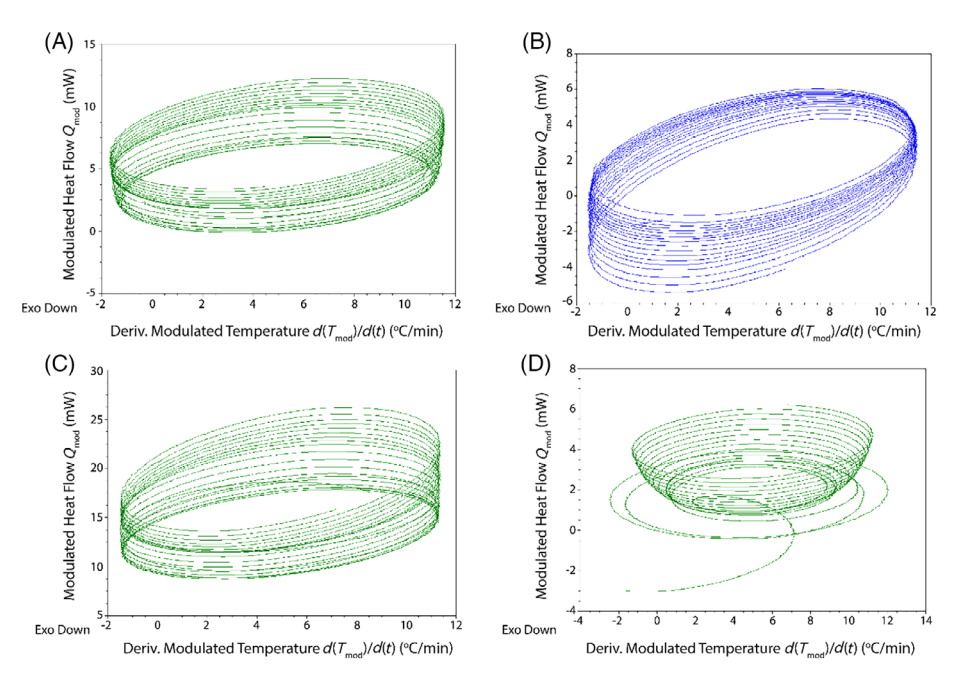


FIGURE 2 A selection of linear Lissajous curves from the studied sodium aluminosilicate (NAS) compositions, specifically for (A) R = .38, (B) R = .9, and (C) R = 1.42, and (D) is an example of a nonlinear response from composition R = 0. Modulation conditions: 5°C/min heating rate, 2°C amplitude, and 120-s period.

the shape is diagonal and the pattern is approximately retraceable, but not completely due to the lower sensitivity of this instrument when compared to traditional MDSCs. All MDSC measurements reported here were done on a TA instrument SDT Discovery 650 with the following parameters: 5°C/min heating rate, a 2°C amplitude, and a 120-second period. These compositions allow for at least four oscillations during the glass transition and an example can be seen in Figure S1. Figure 2D shows an example of a nonlinear response. A parametric study of different heating rates, amplitudes, and periods is planned to determine if there are modulation conditions that better preserve linearity, similar to the parametric study by Bechgaard et al.<sup>28</sup> Since this is a wide range of compositions present, there may also be different modulation conditions that are suitable for different compositions. To the authors' knowledge, this is the first MDSC study of these sodium aluminosilicate glass compositions, so there are no other modulation conditions to compare with.

# 3 | RESULTS AND DISCUSSION

# 3.1 | ICP and XRD

Table 1 shows the theoretical composition calculated from the stoichiometry and used for batching, measured compositions are those obtained from ICP, and the *R* values are calculated from the theoretical and measured compositions. Powder XRD results in Figure 3 showed small

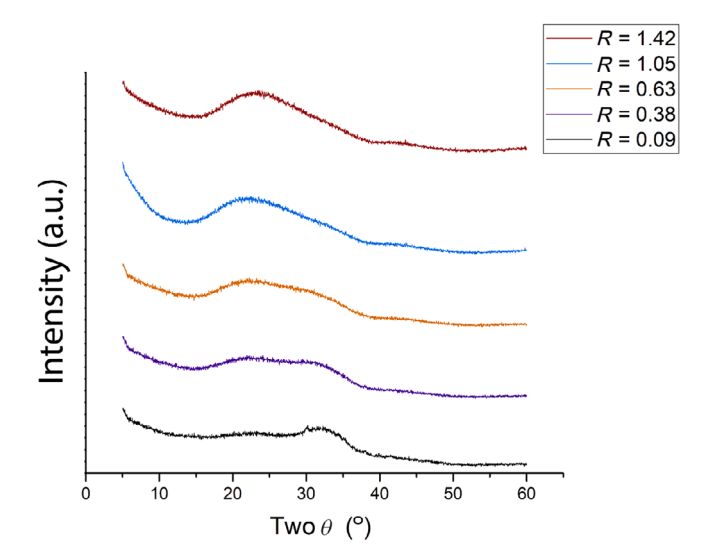


FIGURE 3 X-ray diffraction (XRD) scans for a subset of the sodium aluminosilicate (NAS) compositions. From the bottom up the compositions are R = .09, R = .38, R = .63, R = 1.05, and the topmost curve is R = 1.42. Scans have been stacked vertically for easier comparison.

peaks in the amorphous hump of the compositions with high  $\mathrm{Na_2O}$  content and little to no  $\mathrm{Al_2O_3}$  (R values of 0–.22), indicative of some recrystallization potentially due to the hygroscopic nature of high  $\mathrm{Na_2O}$  content glasses. These results were used to inform which samples to keep in a desiccator under vacuum, especially those that were powdered for ICP and DSC/MDSC analysis.



**TABLE 1** Theoretical compositions and measured compositions for all sodium aluminosilicate glasses in this study with their corresponding *R* ratios.

Theoretical composition (mol%)	Measured composition (mol%)	Theoretical $R = [Al_2O_3]/[Na_2O]$	Measured $R = [Al_2O_3]/[Na_2O]$
$0\mathrm{Al_2O_3}$ –39.2 $\mathrm{Na_2O}$ –61 $\mathrm{SiO_2}$	$0 A l_2 O_3 - 38.2 N a_2 O - 61.8 SiO_2$	.00	.00
$3\mathrm{Al_2O_3}36.2\mathrm{Na_2O}61\mathrm{SiO_2}$	$3.3 \text{Al}_2 \text{O}_3 - 35.3 \text{Na}_2 \text{O} - 61.4 \text{SiO}_2$	.08	.09
$6Al_2O_3$ -33.2 $Na_2O$ - $61SiO_2$	$7Al_2O_3$ -32.3 $Na_2O$ -60.7 $SiO_2$	.18	.22
$8.5 \mathrm{Al_2O_3} - 30.5 \mathrm{Na_2O} - 61 \mathrm{SiO_2}$	$8.4 \text{Al}_2 \text{O}_3 - 30.4 \text{Na}_2 \text{O} - 61.2 \text{SiO}_2$	.28	.28
$10 \text{Al}_2 \text{O}_3 - 29 \text{Na}_2 \text{O} - 61 \text{SiO}_2$	$10.9 {\rm Al_2O_3} - 28.4 {\rm Na_2O} - 60.8 {\rm SiO_2}$	.34	.38
$13\mathrm{Al_2O_3}26\mathrm{Na_2O}61\mathrm{SiO_2}$	$13.4 \mathrm{Al_2O_3} - 25.9 \mathrm{Na_2O} - 60.7 \mathrm{SiO_2}$	.50	.52
$15\text{Al}_2\text{O}_3 - 24\text{Na}_2\text{O} - 61\text{SiO}_2$	$15.1 A l_2 O_3 - 24 N a_2 O - 60.9 SiO_2$	.63	.63
$18\text{Al}_2\text{O}_3$ – $21\text{Na}_2\text{O}$ – $61\text{SiO}_2$	$18.6 \text{Al}_2 \text{O}_3 - 20.7 \text{Na}_2 \text{O} - 60.7 \text{SiO}_2$	.86	.90
$19.5 \text{Al}_2 \text{O}_3 - 19.5 \text{Na}_2 \text{O} - 61 \text{SiO}_2$	$20.4 {\rm Al_2O_3}  19.5 {\rm Na_2O}  60 {\rm SiO_2}$	1.00	1.05
$21\mathrm{Al_2O_3}18\mathrm{Na_2O}61\mathrm{SiO_2}$	$21.7 {\rm Al_2O_3} - 18.4 {\rm Na_2O} - 59.9 {\rm SiO_2}$	1.17	1.18
23Al <sub>2</sub> O <sub>3</sub> –16Na <sub>2</sub> O–61SiO <sub>2</sub>	$23.4 \text{Al}_2 \text{O}_3 - 16.5 \text{Na}_2 \text{O} - 60.2 \text{SiO}_2$	1.44	1.42

Theoretical compositions are calculated according to mol% during batching and measured compositions are those calculated from inductively coupled plasma (ICP).

**TABLE 2** Density measurements and glass transition temperature  $(T_{\rm g})$  from differential scanning calorimetry (DSC) for all glass compositions.

an glass compositions.			
$R = [Al_2O_3]/$ $[SiO_2]$	$T_{ m g}$ (°C) from DSC	Density (g/cm <sup>3</sup> )	
.00	460.25	2.463	
.09	487	2.442	
.22	521.5	2.422	
.28	532.75	2.497	
.38	560.5	2.408	
.52	598.25	2.420	
.63	628.75	2.404	
.90	735	2.454	
1.05	833.75	2.441	
1.18	825.5	2.442	
1.42	826.25	2.443	

Density measurements are averaged from three runs.  $T_{\rm g}$  measurements are averaged from three runs at 10°C/min using both the midpoint method via the TA Trios software and TransitionPy.

# 3.2 | DSC

Glass transition temperatures ( $T_{\rm g}$ s) are given in Table 2 and shown in Figure 6, all taken at 10°C/min with the thermal history previously erased.  $T_{\rm g}$ s were obtained from both the TA midpoint method<sup>64</sup> and the geometric analysis method<sup>65</sup> and were averaged together.  $T_{\rm g}$ s increase with increasing R ratio until reaching a plateau at and above R=1; this suggests that the addition of  ${\rm Al}_2{\rm O}_3$  is increasing the number of constraints in the structure, or that there are fewer atomic degrees of freedom. This occurs until R=1, where  $T_{\rm g}$  flattens out due to the long-range connectivity of the glass being achieved. TCT of NAS glasses suggests

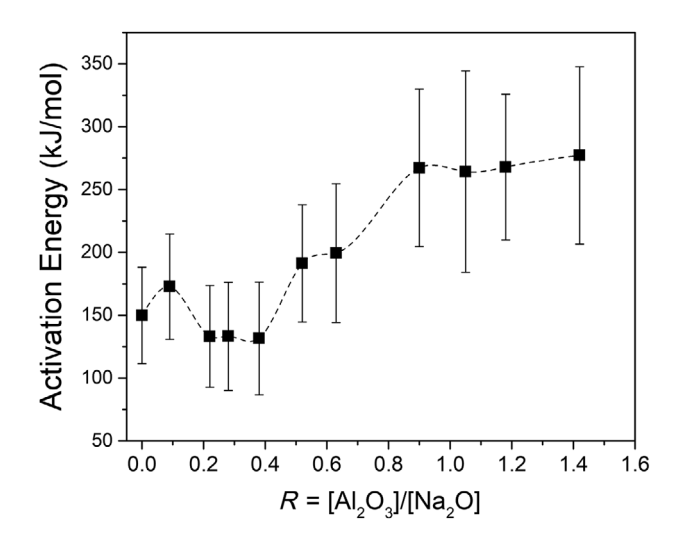


**FIGURE 4** Activation energy calculated from four different heating rates (10, 20, 40, 60°C/min) using the geometric analysis method.

this occurs around R=1 as the number of NBOs reaches zero, bridging oxygens (BOs) reach a maximum and then decrease, and oxygen triclusters (TOs) increase.<sup>69</sup>

The activation energy  $(E_a)$  for enthalpy relaxation is calculated from multiple heating rates (10, 20, 40,  $60^{\circ}$ C/min) using a geometric analysis, expanded upon in the Supporting Information section, and is shown in Figure 4.<sup>65</sup> The activation energy from DSC shows there is a minimum in the relaxation, or a reversibility window, between R = .2 and .4, with the activation energy increasing until about R = .9. After R = .9, the activation energy stabilizes but increases again slightly after R = 1.4. A future goal is to experiment with more ways to calculate the activation energy to see if this trend is consistent across various techniques.



.com/doi/10.1111/ijag.16688 by Pennsylvania State University, Wiley Online Library on [28/10/2024]. See the Terr

itions) on Wiley Online Library for rules of use; OA articles are governed by the applicable Creative Commons

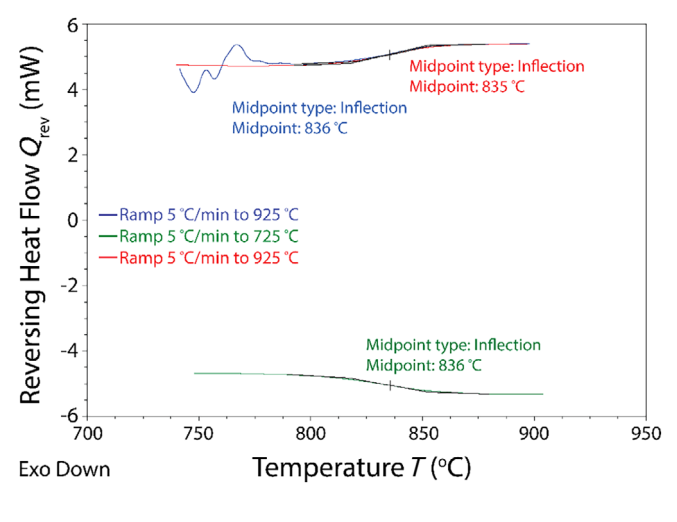


**FIGURE 5** Example reversing heat flow curves from the R = 1.42 composition. The blue curve is the first heating, the green curve is the cooling, and the red curve is the second heating. Modulation conditions:  $5^{\circ}$ C/min heating rate,  $2^{\circ}$ C amplitude, and 120-s period.

## 3.3 | MDSC

While all the modulation conditions were the same for each experiment, the temperature range across compositions is different due to trying to preserve linearity and staying within the glass transition region. For these experiments, the range is chosen to be about 100°C below and about  $100^{\circ}$ C above  $T_{\rm g}$ . The reversing heat flow signals can be another way to determine the  $T_{\rm g}$  of a glass by defining the inflection point of the step in the signal.<sup>39</sup> This can be done for both the heating and cooling curves. Figure 5 shows an example of the reversing heat flow signal and the midpoint method for determining  $T_{\rm g}$  from one NAS composition (R = .22). The average  $T_g$ s from DSC and MDSC are plotted in Figure 6. The MDSC data are averaged from  $T_{\rm g}$ s taken from the two heating scans and the cooling scan. Measuring  $T_g$  from MDSC is considered more accurate than DSC because there is no overlapping signal from the enthalpy relaxation and may be similar to the  $T_{g}$ determined from DSC on the cooling scan.

The enthalpy of relaxation or nonreversing enthalpy ( $\Delta H_{\rm nr}$ ) is calculated by integrating the area under the peak seen in the nonreversing heat flow. <sup>32,40,60</sup> Because the reversing heat flow signal tends to slightly shift at different modulation frequencies and due to the nonreversing heat flow being the difference between the total heat flow and the reversing heat flow signals, a frequency correction is needed to compensate for an overestimation of  $\Delta H_{\rm nr}$ . <sup>32,40,70</sup> This overestimate can be obtained from a cooling cycle and then subtracting it from the first heating cycle, in this case by subtracting the area under the curve of the green cooling scan from the red second heat-

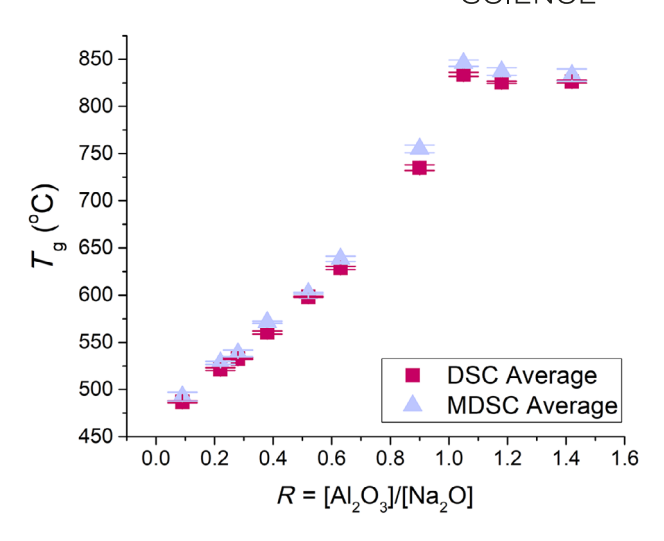


FIGURE 6 Average  $T_{\rm g}$ s from differential scanning calorimetry (DSC) and modulated differential scanning calorimetry (MDSC). MDSC data were averaged for the two heating and the one cooling cycles.

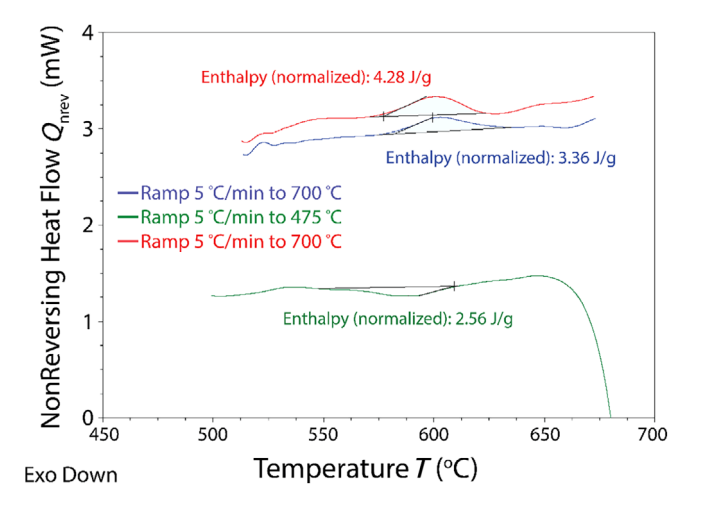


FIGURE 7 Example of the nonreversing heat flow curves from the R=.52 composition. The blue curve is the first heating, the green curve is the cooling, and the red curve is the second heating. The areas under the curves are used to determine the enthalpy of relaxation ( $\Delta H_{\rm nr}$ ). Modulation conditions: 5°C/min heating rate, 2°C amplitude, and 120-s period.

ing scan. Another way to estimate the frequency correction is to have an additional (second) heating cycle and take the difference between  $\Delta H_{\rm nr}$  of the two heating cycles. The idea here is that the second heating records the enthalpy of relaxation of a sample in which the aging time clock has been reset to zero. This technique is more useful to determine the difference in enthalpy relaxation on aging and thus would be beneficial when using samples that have undergone long annealing or aging times. Figure 7 shows an example of the heating–cooling–heating nonreversing

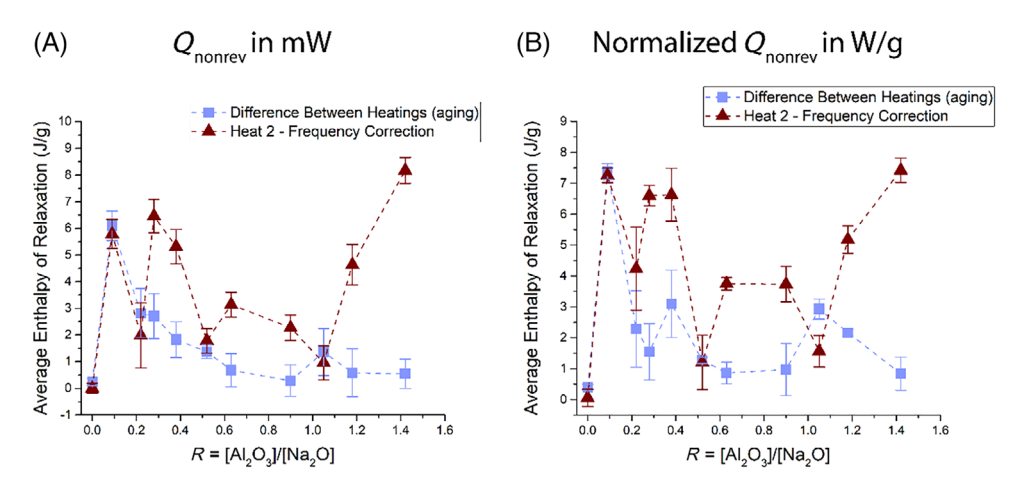


FIGURE 8 Enthalpy of relaxation (J/g) averaged over three different iterations of the area under the curve calculations. The black lines for both plots are the differences between the heating cycles and the blue lines are the frequency correction on cooling subtracted from the second heating scan. (A) Nonreversing heat flow as measured by the instrument in mW. (B) Nonreversing heat flow as measured by the instrument when normalized (W/g).

heat flow with the area under the curve analysis from one glass composition (R = .52).

Figure 8 shows the enthalpy of relaxation for these NAS compositions and compares the results from two different versions of the nonreversing heat flow signal. Figure 8A is the enthalpy of relaxation calculated from the nonreversing heat flow signal in mW, while Figure 8B is the nonreversing heat flow signal normalized in W/g. The area under the curve analysis for each composition was repeated three times to understand the user error that is involved in these measurements, which is especially important as these data are rarely reported with error bars. Each plot shows the enthalpy of relaxation calculated both from the differences in the heating scans and with the thermal histories of the samples erased (second heating) and a frequency correction applied on cooling. Neither of these methods or signals shows a similar minimum found in the activation energy in Figure 4. The overall trends are the same when comparing the mW data versus the normalized (W/g) data, but the two different methods for calculating the enthalpy of relaxation are quite different. The frequency correction method using the second heating does not show a consistent minimum over multiple compositions, while the differences between heating show a potential minimum between R = .6 and 1.0. As mentioned above, the enthalpy of relaxation from this nonreversing heat flow technique has not matched the reversibility windows found from activation energy data. This technique is also not well standardized, and error is rarely reported for the enthalpy of relaxation. More work is needed to study this technique on oxide glasses, especially those with high  $T_{\rm g}$ s.

# 4 | CONCLUSIONS

This study measured activation energy and enthalpy of relaxation for a wide range of sodium aluminosilicate compositions with  $R = [Al_2O_3]/[Na_2O]$  values ranging from 0 to 1.42. XRD plots, ICP measurements, density values, and  $T_g$  from DSC were reported for each composition. Traditional DSC scans were used to calculate the activation energy and relaxation time. This is the first study using the TA SDT 650 for MDSC on NAS glasses, and it was found that the modulation conditions of 5°C/min heating rate, a 2°C amplitude, and a 120-s period allowed the system to keep a linear response, as seen in the Lissajous curves. The reversing heat flow was analyzed to provide a more accurate  $T_g$  measurement, while the nonreversing heat flow was used to calculate the enthalpy of relaxation. The enthalpy of relaxation analysis was performed three times, allowing for a better idea of the user error involved in this type of measurement, which is not normally reported in the literature. Our results showed that the reversibility windows between the activation energy and enthalpy of relaxation did not match to the same compositions. Both points demonstrate that additional work needs to be done to determine whether the nonreversing heat flow method is useful for high  $T_{\rm g}$  oxide glasses and to standardize the process for finding the areas under the curves and report. Future work in this area will include a parametric study of MDSC conditions for these sodium aluminosilicate glasses, comparing MDSC results between two different instruments (TA SDT 650 and Netzsch Jupiter STA), and completing the complex heat capacity MDSC analysis for more insights into the relaxation behavior of these glasses.



### ACKNOWLEDGMENTS

The authors would like to acknowledge Laura J. Liermann for collecting ICP data and Nichole M. Wonderling and Ellery Schlorff of the Penn State Materials Characterization Lab for performing XRD. We are also thankful for valuable discussion with Aaron Bossen and Katie Kirchner at Penn State and advice from Ozgur Gulbiten at Corning Inc. We are grateful for funding from the National Science Foundation (DMR 1928546).

### ORCID

Brittney M. Hauke https://orcid.org/0000-0002-4175-8569

John C. Mauro https://orcid.org/0000-0002-4319-3530

### REFERENCES

- 1. Varshneya AK. Chemical strengthening of glass: lessons learned and yet to be learned. Int J Appl Glass Sci. 2010;1(2):131–42. https://doi.org/10.1111/j.2041-1294.2010.00010.x
- Mauro JC, Ellison AJ, Pye LD. Glass: the nanotechnology connection. Int J Appl Glass Sci. 2013;4(2):64–75. https://doi.org/10. 1111/ijag.12030
- Zanotto ED, Mauro JC. The glassy state of matter: its definition and ultimate fate. J Non-Cryst Solids. 2017;471:490–95. https:// doi.org/10.1016/j.jnoncrysol.2017.05.019
- Varshneya AK, Mauro JC. Fundamentals of inorganic glasses.
   3rd ed. Elsevier; Cambridge, MA, US, 2019.
- Ellison A, Cornejo IA. Glass substrates for liquid crystal displays. Int J Appl Glass Sci. 2010;1(1):87–103. https://doi.org/10.1111/j. 2041-1294.2010.00009.x
- Boesch L, Napolitano A, Macedo PB. Spectrum of volume relaxation times in B<sub>2</sub>O<sub>3</sub>. J Am Ceram Soc. 1970;53(3):148–53. https://doi.org/10.1111/j.1151-2916.1970.tb12057.x
- 7. Gulbiten O, Mauro JC, Lucas P. Relaxation of enthalpy fluctuations during sub- $T_g$  annealing of glassy selenium. J Chem Phys. 2013;138(24):244504. https://doi.org/10.1063/1.4811488
- 8. Potuzak M, Welch RC, Mauro JC. Topological origin of stretched exponential relaxation in glass. J Chem Phys. 2011;135(21):214502. https://doi.org/10.1063/1.3664744
- Welch RC, Smith JR, Potuzak M, Guo X, Bowden BF, Kiczenski TJ, et al. Dynamics of glass relaxation at room temperature. Phys Rev Lett. 2013;110(26):265901. https://doi.org/10.1103/ PhysRevLett.110.265901
- Mauro JC, Philip CS, Vaughn DJ, Pambianchi MS. Glass science in the United States: current status and future directions. Int J Appl Glass Sci. 2014;5(1):2–15. https://doi.org/10.1111/ijag.12058
- Varshneya AK, Olson GA, Kreski PK, Gupta PK. Buildup and relaxation of stress in chemically strengthened glass. J Non-Cryst Solids. 2015;427:91–97. https://doi.org/10.1016/j. jnoncrysol.2015.07.037
- 12. Sane AY, Cooper AR. Stress buildup and relaxation during ion exchange strengthening of glass. J Am Ceram Soc. 1987;70(2):86–89. https://doi.org/10.1111/j.1151-2916.1987.tb04934.x
- Lucas P, King EA, Gueguen Y, Sangleboeuf J-C, Keryvin V, Erdmann RG, et al. Correlation between thermal and mechanical relaxation in chalcogenide glass fibers. J Am Ceram

- Soc. 2009;92(9):1986–92. https://doi.org/10.1111/j.1551-2916.2009. 03150.x
- Mysen BO. Structure and properties of silicate melts. Amsterdam: New York: Elsevier: 1988.
- Mysen BO, Virgo D, Kushiro I. The structural role of aluminum in silicate melts—a Raman spectroscopic study at 1 atmosphere. Am Mineral. 1981;66(7–8):678–701.
- Xiang Y, Du J, Smedskjaer MM, Mauro JC. Structure and properties of sodium aluminosilicate glasses from molecular dynamics simulations. J Chem Phys. 2013;139(044507):1–18.
- 17. Le Losq C, Neuville DR, Florian P, Henderson GS, Massiot D. The role of Al<sup>3+</sup> on rheology and structural changes in sodium silicate and aluminosilicate glasses and melts. Geochim Cosmochim Acta. 2014;126:495–517. https://doi.org/10.1016/j.gca. 2013.11.010
- McKeown DA, Galeener FL, Brown GE. Raman studies of Al coordination in silica-rich sodium aluminosilicate glasses and some related minerals. J Non-Cryst Solids. 1984;68(2):361–78. https://doi.org/10.1016/0022-3093(84)90017-6
- Onorato PIK, Alexander MN, Struck CW, Tasker GW, Uhlmann DR. Bridging and nonbridging oxygen atoms in alkali aluminosilicate glasses. J Am Ceram Soc. 1985;68(6):C-148-C-150. https://doi.org/10.1111/j.1151-2916.1985.tb15223.x
- Thomsen RM, Skibsted J, Yue Y. The charge-balancing role of calcium and alkali ions in per-alkaline aluminosilicate glasses. J Phys Chem B. 2018;122(12):3184–95. https://doi.org/10.1021/acs. jpcb.7b12437
- Zirl DM, Garofalini SH. Structure of sodium aluminosilicate glasses. J Am Ceram Soc. 1990;73(10):2848–56. https://doi.org/ 10.1111/j.1151-2916.1990.tb06685.x
- Welch RS, Astle S, Youngman RE, Mauro JC. High-coordinated alumina and oxygen triclusters in modified aluminosilicate glasses. Int J Appl Glass Sci. 2022;13(3):388–401. https://doi.org/ 10.1111/jiag.16565
- 23. Riebling EF. Structure of sodium aluminosilicate melts containing at least 50 mole % SiO<sub>2</sub> at 1500°C. J Chem Phys. 1966;44(8):2857–65. https://doi.org/10.1063/1.1727145
- 24. Neuville DR, Cormier L, Flank, A-M, Briois V, Massiot D. Al speciation and Ca environment in calcium aluminosilicate glasses and crystals by Al and Ca K-edge X-ray absorption spectroscopy. Chem Geol. 2004;213:153–63.
- 25. Toplis MJ, Dingwell DB, Lenci T. Peraluminous viscosity maxima in  $Na_2O-Al_2O_3$ -SiO<sub>2</sub> liquids: the role of triclusters in tectosilicate melts. Geochim Cosmochim Acta. 1997;61(13):2605–12. https://doi.org/10.1016/S0016-7037(97)00126-9
- 26. Welch RS, Lee K-H, Wilkinson CJ, Ono M, Bragatto CB, Mauro JC. Topological hardening through oxygen triclusters in calcium aluminosilicate glasses. J Am Ceram Soc. 2021;104(12):6183–93. https://doi.org/10.1111/jace.18032
- Liu Z, Hu Y, Li X, Song W, Goyal S, Micoulaut M, et al. Glass relaxation and hysteresis of the glass transition by molecular dynamics simulations. Phys Rev B. 2018;98(10):104205. https:// doi.org/10.1103/physrevb.98.104205
- Bechgaard TK, Gulbiten O, Mauro JC, Smedskjaer MM. Parametric study of temperature-modulated differential scanning calorimetry for high-temperature oxide glasses with varying fragility. J Non-Cryst Solids. 2018;484:84–94. https://doi.org/10.1016/j.jnoncrysol.2018.01.022



- 29. Bechgaard TK, Gulbiten O, Mauro JC, Hu Y, Bauchy M, Smedskjaer MM. Temperature-modulated differential scanning calorimetry analysis of high-temperature silicate glasses. arXiv:180501433 [cond-mat]. 2018.
- Stebbins JF, Ellsworth SE. Temperature effects on structure and dynamics in borate and borosilicate liquids: high-resolution and high-temperature NMR results. J Am Ceram Soc. 1996;79(9):2247–56. https://doi.org/10.1111/j.1151-2916.1996.tb08969.x
- 31. Lucas P, King EA, Gulbiten O, Yarger JL, Soignard E, Bureau B. Bimodal phase percolation model for the structure of Ge-Se glasses and the existence of the intermediate phase. Phys Rev B. 2009;80(21):214114. https://doi.org/10.1103/PhysRevB.80. 214114
- Zheng Q, Zhang Y, Montazerian M, Gulbiten O, Mauro JC, Zanotto ED, et al. Understanding glass through differential scanning calorimetry. Chem Rev. 2019;119(13):7848–939. https:// doi.org/10.1021/acs.chemrev.8b00510
- Jiang Z, Imrie CT, Hutchinson JM. An introduction to temperature modulated differential scanning calorimetry (TMDSC): a relatively non-mathematical approach. Thermochim Acta. 2002;387(1):75–93. https://doi.org/10.1016/S0040-6031(01)00829-2
- Reading M, Elliott D, Hill VL. A new approach to the calorimetric investigation of physical and chemical transitions. J Therm Anal. 1993;40(3):949–55. https://doi.org/10.1007/BF02546854
- 35. Reading M, Luget A, Wilson R. Modulated differential scanning calorimetry. Thermochim Acta. 1994;238:295–307. https://doi.org/10.1016/S0040-6031(94)85215-4
- Gobrecht H, Hamann K, Willers G. Complex plane analysis of heat capacity of polymers in the glass transition region. J Phys E: Sci Instrum. 1971;4(1):21. https://doi.org/10.1088/0022-3735/4/1/ 004
- 37. Birge NO, Nagel SR. Specific-heat spectroscopy of the glass transition. Phys Rev Lett. 1985;54(25):2674–77. https://doi.org/10. 1103/PhysRevLett.54.2674
- 38. Chbeir R, Welton A, Burger M, Chakravarty S, Dash S, Bhosle S, et al. Glass transition, topology, and elastic models of Se-based glasses. J Am Ceram Soc. 2023;106(6):3277–302. https://doi.org/10.1111/jace.19003
- 39. Gulbiten O. An investigation of dynamic processes in selenium based chalcogenide glasses. PhD dissertation. The University of Arizona; 2014.
- 40. Chen P, Boolchand P, Georgiev DG. Long term aging of selenide glasses: evidence of sub- $T_{\rm g}$  endotherms and pre- $T_{\rm g}$  exotherms. J Phys: Condens Matter. 2010;22(6):065104. https://doi.org/10. 1088/0953-8984/22/6/065104
- 41. Boolchand P, Feng X, Bresser WJ. Rigidity transitions in binary Ge–Se glasses and the intermediate phase. J Non-Cryst Solids. 2001;293–295:348–56. https://doi.org/10.1016/S0022-3093(01)00867-5
- 42. Vaills Y, Qu T, Micoulaut M, Chaimbault F, Boolchand P. Direct evidence of rigidity loss and self-organization in silicate glasses. J Phys: Condens Matter. 2005;17(32):4889–96. https://doi.org/10. 1088/0953-8984/17/32/003
- 43. Shatnawi MTM, Farrow CL, Chen P, Boolchand P, Sartbaeva A, Thorpe MF, et al. Search for a structural response to the intermediate phase in Ge<sub>x</sub>Se<sub>1-x</sub> glasses. Phys Rev B. 2008;77(9):094134. https://doi.org/10.1103/PhysRevB.77.094134

- 44. Sreevidya Varma G, Das C, Asokan S. Evidence of an intermediate phase in a quaternary Ag bearing telluride glass system using alternating DSC. Solid State Commun. 2014;177:108–12. https://doi.org/10.1016/j.ssc.2013.10.003
- Micoulaut M. Amorphous materials: properties, structure, and durability: constrained interactions, rigidity, adaptative networks, and their role for the description of silicates. Am Mineral. 2008;93(11–12):1732–48. https://doi.org/10.2138/am.2008.2903
- Rompicharla K, Novita DI, Chen P, Boolchand P, Micoulaut M, Huff W. Abrupt boundaries of intermediate phases and space filling in oxide glasses. J Phys: Condens Matter. 2008;20(20):202101. https://doi.org/10.1088/0953-8984/20/20/202101
- Chakraborty S, Boolchand P, Malki M, Micoulaut M. Designing heavy metal oxide glasses with threshold properties from network rigidity. J Chem Phys. 2014;140(1):014503. https://doi.org/ 10.1063/1.4855695
- 48. Matsuda Y, Fukawa Y, Ike Y, Kodama M, Kojima S. Dynamic specific heat, glass transition, and non-Debye nature of thermal relaxation in lithium borate glasses. J Phys Soc Jpn. 2008;77(8):084602. https://doi.org/10.1143/JPSJ.77.084602
- 49. Mandal A, Gogi VK, Mohanty C, Chbeir R, Boolchand P. Emerging role of local and extended range molecular structures on functionalities of topological phases of  $(Na_2O)_x(P_2O_5)_{100-x}$  glasses using Raman scattering and modulated DSC. Int J Appl Glass Sci. 2021;12(1):89–110. https://doi.org/10.1111/ijag.15809
- Bechgaard TK, Gulbiten O, Mauro JC, Yue Y, Bauchy M, Smedskjaer MM. Liquid fragility determination of oxide glassformers using temperature-modulated DSC. Int J Appl Glass Sci. 2019;10(3):321–29. https://doi.org/10.1111/ijag.13105
- Schawe JEK. Principles for the interpretation of modulated temperature DSC measurements. Part 1. Glass transition. Thermochim Acta. 1995;261:183–94. https://doi.org/10.1016/0040-6031(95)02315-S
- Schawe JEK. Principles for the interpretation of temperature-modulated DSC measurements. Part 2: a thermodynamic approach. Thermochim Acta. 1997;304–305:111–19. https://doi.org/10.1016/S0040-6031(97)00203-7
- Schawe JEK. A comparison of different evaluation methods in modulated temperature DSC. Thermochim Acta. 1995;260:1–16. https://doi.org/10.1016/0040-6031(95)90466-2
- 54. Weyer S, Hensel A, Schick C. Phase angle correction for TMDSC in the glass-transition region. Thermochim Acta. 1997;304–305:267–75. https://doi.org/10.1016/S0040-6031(97)00180-9
- 55. Wunderlich B, Jin Y, Boller A. Mathematical description of differential scanning calorimetry based on periodic temperature modulation. Thermochim Acta. 1994;238:277–93. https://doi.org/10.1016/S0040-6031(94)85214-6
- Fukawa Y, Matsuda Y, Kawashima M, Kojima S. Determination of complex-specific heat and fragility of sodium borate glasses by temperature-modulated DSC. J Therm Anal Calorim. 2010;99(1):39–44. https://doi.org/10.1007/s10973-009-0522-5
- Matsuda Y, Fukawa Y, Kawashima M, Kojima S. Fragility variation of lithium borate glasses studied by temperaturemodulated DSC. AIP Conf Proc. 2008;982(1):207–10. https://doi. org/10.1063/1.2897785
- 58. Micoulaut M. Relaxation and physical aging in network glasses: a review. Rep Prog Phys. 2016;79(6):066504. https://doi.org/10.1088/0034-4885/79/6/066504



- 59. Boolchand P. Intermediate phases, reversibility windows, stressfree and non-aging networks, and strong liquids. Chalcogenide Lett. 2006;3(2):29–31.
- 60. Gogi VK, Mandal A, Welton A, Bhosle S, Chakraborty S, Gunasekera K, et al. Linking molecular origin of melt fragility index with topological phases of network glasses. J Non-Cryst Solids. 2024;631:122920. https://doi.org/10.1016/j.jnoncrysol.2024.122920
- Mauro JC. Topological constraint theory of glass. Am Ceram Soc Bull. 2011;90(4):7.
- 62. Bauchy M. Topological constraint theory and rigidity of glasses. In: Sattler KD, editor. 21st century nanoscience—a handbook. 1st ed. Boca Raton, FL: CRC Press; 2019. p. 13-1–13-20. https://doi.org/10.1201/9780367333003-13
- Thompson M, Walsh JN. Inductively coupled plasma mass spectrometry. In: Thompson M, Walsh JN, editors. Handbook of inductively coupled plasma spectrometry. Boston, MA: Springer US; 1989. p. 238–69. https://doi.org/10.1007/978-1-4613-0697-9\_11
- 64. E37 Committee. Test method for assignment of the glass transition temperatures by differential scanning calorimetry. ASTM International; 2014. https://www.astm.org/e1356-08r14.html
- 65. Mancini M, Sendova M, Mauro JC. Geometric analysis of the calorimetric glass transition and fragility using constant cooling rate cycles. Int J Appl Glass Sci. 2021;12(3):348–57. https://doi.org/10.1111/ijag.16073
- 66. Boller A, Schick C, Wunderlich B. Modulated differential scanning calorimetry in the glass transition region. Thermochim Acta. 1995;266:97–111. https://doi.org/10.1016/0040-6031(95)02552-9

- 67. Wunderlich B, Boller A, Okazaki I, Kreitmeier S. Linearity, steady state, and complex heat capacity in modulated differential scanning calorimetry. Thermochim Acta. 1996;282–283:143–55. https://doi.org/10.1016/0040-6031(95)02808-0
- 68. Tomozawa M, Ito S, Molinelli J. Hygroscopicity of glasses with high water content. J Non-Cryst Solids. 1984;64(1):269–78. https://doi.org/10.1016/0022-3093(84)90222-9
- Ching E, Bauchy M. Topological origins of flexibility and internal stress in sodium aluminosilicate glasses. arXiv: Materials Science. 2018.
- 70. Guo X, Mauro JC, Allan DC, Yue Y. On the frequency correction in temperature-modulated differential scanning calorimetry of the glass transition. J Non-Cryst Solids. 2012;358(14):1710–15. https://doi.org/10.1016/j.jnoncrysol.2012.05.006

### SUPPORTING INFORMATION

Additional supporting information can be found online in the Supporting Information section at the end of this article.

**How to cite this article:** Hauke BM, Mauro JC. Enthalpy relaxation of sodium aluminosilicate glasses from thermal analysis. Int J Appl Glass Sci. 2024;1–11. https://doi.org/10.1111/ijag.16688

